QUT Digital Repository:
http://eprints.qut.edu.au/

QUT

This is the author's version published as:

Frost, Ray L., Blain, Paul, Martens, Wayde N., & Yang, Dongjiang (2011) *Sodium niobate adsorbents doped with tantalum (TaV) for the removal of bivalence radioactive ions in waste waters*. Journal of Colloid and Interface Science, 356(1), pp. 240-247.

Sodium Niobate Adsorbents Doped with Tantalum (Ta^V) for the Removal of Bivalence Radioactive Ions in Waste Waters

Blain Paul, Dongjiang Yang,Wayde N. Martens, Ray L. Frost*

Discipline of Chemistry, Queensland University of Technology, Brisbane, Qld 4001,

Australia, Email*: r.frost@qut.edu.au, Fax: +61 7 3138 1804

Abstract

Sodium niobates doped with different amount of tantalum (Ta^V) were prepared via thermal reaction process. It was found pure nanofibril and bar-like solids can be obtained when tantalum was introduced into the reaction system. For the well-crystallized fibril solids, the Na$^+$ ions are difficult to be exchanged, and the radioactive ions such as Sr^{2+} and Ra^{2+} ions just deposit on the surface of the fibers during the sorption process, resulting in lower sorption capacity and distribution coefficients (K$_d$)`. However, the bar-like solids are poorly-crystallized and have lots of exchangeable Na$^+$ ions. They are able to remove highly hazardous bivalent radioactive isotopes such as Sr^{2+} and Ra^{2+} ions. Even in the presence of lots of Na$^+$ ions, they also have higher K$_d$. More importantly, such sorption finally intelligently triggers considerable collapse of the structure, resulting in the entrapment of the toxic bivalent cations permanently in the solids so that they can be safely disposed. This study highlights new opportunities for the preparation of Nb-based adsorbents to efficiently remove the toxic radioactive ions from contaminated water.

1. Introduction

While investigating the contamination of the environment by radioactive ions from the heap-leach residues of the uranium mining industry (such as $^{226}Ra^{2+}$ ions) and while addressing the by-product of nuclear fission reaction (such as $^{90}Sr^{2+}$) as well as the leakage of the nuclear reactors; one should not be daunted, extensive research is underway to develop advanced technologies for the elimination of hazardous radioactive ions from water [1-7].

In fact, different methods are used to remove radioactive metal ions from waste water such as ion exchange and adsorption [8-11]. Ion exchange processes are selective, very effective and are able to remove very low levels of metal ions from solutions [12-16]. However, the development of materials with a high level of efficiency and selectivity by an order of magnitude is still in its infancy. In fact, the ever more sophisticated future versions of scavenger solids also demands a framework capable of binding guests such as radioactive ions inside irreversibly, without any leaching as a safe storage material [1].

Environmental remediation efforts have been somewhat successful after the discovery of the following materials. Organic resins are unlikely to compete with zeolites and other clay absorbents due to their limited long-term stability under high radiation conditions as well as due to their high cost [4]. Moreover, the inability of organic resins to maintain permanent thermal, chemical, mechanical and radiation stabilities as well as their inability to avoid structural rearrangements upon guest exchange has been an obvious drawback [17, 18]. In spite of the promise for selectivity and high radiation stability, zeolite and clays are high pH responsive materials [19]. However, synthetic inorganic cation-exchangers provide the best examples of practical success. One of the first examples of such a solid was synthetic mica, which has an efficiency

that is larger than the efficiency of any natural inorganic exchangers [3, 5]. Another example is a γ-zirconium phosphate framework [2]. Very recently developed titanate [1, 20, 21] and niobate [6, 7] solids has exhibited a high storage capacity as well as a high selectivity. Moreover, synthetic inorganic cation exchangers appear to be particularly suitable for immobilizing radioactive ions and thus mitigate toxicity from water [3, 5]. It can be observed that these reinforced solids favour the uptake of radioactive ions not only at distinctly lower concentrations, but also with a considerably higher degree of selectivity [2-7, 21]. These new types of synthetic cation exchangers, which can act as host materials, involve the immobilization of the nuclear waste that is being developed; however, the commercial viability of the resultant solids is often limited because of the high production cost. Clearly, although suitable compounds have not yet been found and numerous challenges remain, this slowly advancing area will deliver exciting developments in future. The synthesis of an efficient material also constitutes other challenges such as low yield, low speed and low reproducibility, which although not new, however remains unsolved. We have recently begun to fabricate structures with nanometric precision in order to incorporate several of these desirable features into one solid-stage material.

Recently, sodium niobate molecular sieves doped with Ti/Zr -IV were synthesized by hydrothermal treatment [6, 7]. It was found that the sodium niobate molecular sieves can selectively adsorb Sr^{2+} ions from highly concentrated Na^+ aqueous solutions [22]. A structural evolution during the reaction between the Nb_2O_5 powder and the concentrated aqueous NaOH solution under hydrothermal conditions was also reported by our group [23], which provides a marvelous opportunity for the further growth of the niobate community.

Herein, a new family of Ta(V) doped sodium niobates were synthesised using chloride precursors via the reported hydrothermal reaction at 165 ºC. The Ta:Nb ratio in the resultant product is directly correlated with the precursor molar ratio for the range of 0 – 10% Ta:Nb. Within this composition range, bar-like solids with poor crystalline and well-crystallized fibers (2%) are formed based on powder X-ray diffraction (XRD) and scanning electron microscopy (SEM). The bar-like solids possess excellent abilities to exchange with the radioactive Sr^{2+} and Ra^{2+} (Ba^{2+}) ions in water. More importantly, by monitoring the structural change before and after adsorption with XRD and Raman spectroscopy, we are able to determine the structural collapse of bar-like solids due to the toxic bivalent ions that are exchanged with Na^+ ions in the solids. The structural collapse induced by the ion-exchange process entraps the radioactive ions in the adsorbents permanently, so that the hazardous radioactive contaminants can be safely disposed of. This is significant research on efficient adsorbents for the removal of radioactive ions from water.

2. Experimental Section

2.1 Sample preparation

All of the chemicals used were reagent grade or better and were provided by the Sigma Chemical Cooperation. Ta^V doped sodium niobates were synthesised starting with the $NbCl_5$ and the $TaCl_5$ precursors. The incorporation of tantalum into the niobates was carried out by dissolving 0.5 g of $NbCl_5$ in 20 ml of a dry propan-2-ol mixed with a different weight ratio of tantalum, which was in the range from 0, 0.5, 1, 2, 5 to 10% under nitrogen flow. When the $NbCl_5$ dissolved in propan-2-ol was used as a Nb precursor, a yellow precipitate initially appeared after the propan-2-ol addition, which disappeared again after stirring for 20 min. A transparent solution was obtained after 24 h of stirring, to which 10 ml of distilled water was carefully added in

a dropwise manner and finally a transparent gel was formed after 24 h. The precipitates were separated by filtration and washed with deionised water several times in order to remove the chlorides. The resulting mixture of oxides was then reacted with 10 M of sodium hydroxide under hydrothermal conditions. The syntheses of Ta incorporated niobates were prepared in specially designed autoclaves at 165 ºC for 2 h. The solid products in the reaction mixture were recovered by filtration, washed several times with deionized water, then with ethanol once, and finally dried at 100 ºC for 24 h. These syntheses were perfectly reproducible.

2.2 Adsorption experiments

It should be noted that radioactive strontium and radium ions are highly hazards in nature, therefore due to safety reasons all of the studies were carried out in a non-radioactive environment. In a further compilation of relevant literature, we found that Ba^{2+} ions (1.36 Å) have a extremely similar ionic radius to radioactive $^{226}Ra^{2+}$ ions (1.43 Å) as well as possessing a similar ion exchange property [24]. Therefore, there is a significant incentive to use barium as a representative of radium in order to mimic all of the properties of radium except for the radioactivity. In such a situation we also used non radioactive strontium. The sorption isotherm of M^{2+} ions ($M^{2+} = Sr^{2+}$ and Ba^{2+}) were determined by equilibrating 10 mg of adsorbent in 50 ml of $SrCl_2$ or $BaCl_2$ solutions at concentrations between 0 to 200 ppm for 24 h at room temperature. In fact, the deposition of a carbonate such as $SrCO_3$ or $BaCO_3$ is often accompanied on the surface of the sorbent at a high pH level. In order to avoid this tendency the pH of the solution was adjusted to a range between 6 and 7 using diluted HCl solution during the adsorption process.

The distribution coefficients (K_d) were determined by the analysis of the filtered solution [3, 6, 25] and were calculated from the expression:

$$K_d = \frac{C_o - C_{eq}}{C_{eq}} \frac{V}{m} \qquad (1)$$

where C_o is the initial concentration (mg/ml), C_{eq} is the concentration after equilibrating (mg /ml), V is the solution volume (ml) and m is the mass of exchanger (g). The K_d represents the ratio of the amount of barium or strontium adsorbed per gram of solid to the amount of strontium or barium remaining per milliliter of the solution, and thus has units mL/g.

2.3 Characterization

Niobate materials were characterized by scanning electron microscopy (SEM), power X-ray diffraction (XRD), Raman spectra, and diffuse reflectance UV-visible (DR-UV-Vis) spectroscopy techniques prior to and after adsorption experiments. Raman spectra were measured by the presentation of the dehydrated sample on a stainless steel slide and the spectra were collected on Renishaw 1000 Olympus BHSM microscope system equipped with 10× and 50× objectives, which was fitted with a monochromator, a filter system and a charge coupled device (CCD). The excited source was a Renishaw doubled laser diode-pumped Nd-YAG emitting at a wavelength of 633 nm at a resolution of 4 cm^{-1} in the range between 100 and 4000 cm^{-1}. Repeated acquisition using the highest magnification was accumulated to improve the signal-to-noise ratio. Spectra were calibrated using the 520.5 cm^{-1} line of a silion wafer. SEM images were taken with an FEI Quanta 200 scanning electron microscope. XRD patterns of the sample powder were recorded on a Siemens D5000 diffractometer equipped with a graphite monochromator. Cu Kα radiation and a fixed power source (40 kV and 40 mA) were used. The data were collected over a 2θ range between 4 and 75°, at a scanning rate of 2.5°/ min. The diffuse reflectance UV-visible (DR-UV-Vis) spectra of the samples were acquired with the Varian Cary 5E UV-Vis-

NIR spectrophotometer. The concentration of M^{2+} in the aqueous solution was analyzed by ion coupled plasma (ICP) technique using a Varian Liberty 200 ICO emission spectrometer.

3. Results and discussion

3.1 Particle morphology

The SEM images of the samples in Figure 1 illustrate the interesting morphological changes of the solids by incorporating Ta^V in various percentages into the frame work structures. Without any doping, the niobate product displays grain morphology of several micrometers in size (Figure 1a), which is similar to our reported early-stage niobate samples prepared at 180 ℃ by the use of Nb_2O_5 as a reagent [26]. With the introduction of 0.5% Ta^V, long bar-like particles with a length of tens of micrometers were obtained (Figure 1b).

A few fibres with a length of tens of micrometers and a width of several micrometers were formed at the expense of the bars were observed in 1% Ta^V doped sample (Figure 1c). As the doping amount of Ta^V increased to 2%, highly uniform fibril morphology was obtained (Figure 1d). It has also been observed that a further increase in the Ta^V amount leads to a disappearance of the fibre structure. For example, when the doped Ta^V amount had reached a level of 5% and 10%, the fibre phase had almost totally disappeared and only long bar-like particles were retained (Figure 1e and 1f). This result suggests that a change in the amount of Ta^V, was found to cause a change in the morphology as well as in the overall crystalline nature of the products.

3.2 XRD Patterns and Raman Spectra

The XRD patterns of the solids are presented in Figure 2a. For the pure fibre phase (2% Ta^V), the reflection peaks in the XRD pattern are narrow and have a high intensity, indicating well-crystallized fibres were formed. The crystal parameters are the space group C2/c, a = 16.984 Å; b = 5.0245 Å; c = 16.432 Å; β= 113.88°. These results fit in well with recent reported work [22]. However, the reflection peaks in the XRD patterns of other samples are broad and have a low intensity, this means that less crystallinity exists in these bar-like solids (Figure 1). The Raman spectra of samples have features typical of niobate phases [27-32]. Similar to the XRD patterns of the samples, the Raman spectrum of the pure fibre niobate is different from those of the bar-like solids (Figure 2b). For the bar-like solids, the strong peak at 897 cm^{-1} is assigned to the short Nb=O stretching mode (A_{1g}), and an intrinsic band at 851 cm^{-1} is due to the vibration of the short Nb=O bond (~1.8 Å). A weak band was also found that at 567cm^{-1}; this peak was found to correspond to the E_g mode arising from stretching the vibration of Nb-O-Nb [23]. The Raman lines at 290 and 220 cm^{-1} can be assigned as the A_{1g} and T_{2g} modes of the bar-like niobate phase, respectively. The A_{1g} mode at 290 cm^{-1} arising from the breathing vibration of the long Nb–O bond and T_{2g} mode at 220 cm^{-1} reveals the bending vibration of the Nb–O–Nb (bridging O atom) [30]. For the 2% Ta doped sample, new bands at 461 and 641 cm^{-1} were observed. The former corresponds to the bridge Nb–O stretching mode together with the T_{2g} symmetry and the latter is also probably associated with the edge-sharing of the NbO_6 octahedra [23]. The other obvious change is due to the fact that the band has disappeared at 570 cm^{-1}. Furthermore, the A_{1g} band observed at 288 cm^{-1} in the spectra of poor-crystallized solids is split into two weak bands at 270 and 305 cm^{-1},

respectively. The bands at 897 and 851 cm^{-1} are shifted to 883 and 842 cm^{-1}, respectively. These spectra are basically similar to those of our previously reported sodium niobates [23]. However, no Raman bands of crystalline Ta_2O_5 were observed at 105, 253 and 627 cm^{-1} in any of the solids [33, 34].

According to our previous work, the bar-like solids in the less crystalline phase are mainly composed of intermediate with edge-sharing $Nb_6O_{19}^{8-}$ units. The well-crystallized fibril solids are composed of edge-sharing NbO_6 octahedral units [23]. Note that the central Nb atom is octahedrally coordinated by six oxygen atoms in each unit. Clearly, these octahedra form the primary building blocks of different morphologies by sharing corners as well as occasionally sharing edges and faces depending on the hydrothermal conditions. In our tantalum doped hydrothermal syntheses of niobates, the doped elements take part in the coordination entities. As a result those metal cations influence the build up of the polyhedra which were connected in the sequence. All of the hydrothermal preparations have a Nb:Ta ratio within a relatively narrow range. Too much or too little tantalum in these reactions gives rise to bar like-solids that do not crystallize well. However, the detailed mechanism herein is not clear although these syntheses are perfectly reproducible.

3.3 UV-Visible Spectra

Figure 3 presents the UV-vis spectra of various niobate products. According to the early reports [23, 35-37], oxygen to metal charge transfer bands can be influenced by the transition metal ion as well as by the number of oxygen atom surrounding it. Therefore, the changes in UV−vis absorbance upon doping are consistent with the types of transition metal oxide configurations present in the sample. Pure Ta_2O_5 exhibits a main adsorption band at 270 nm which is from the octahedral configuration

of Ta^{5+} ion [38]. As anticipated, 2% of the Ta^V doped sample with pure fibril morphology and the well-crystallized phase have weak but distinguishable charge-transfer transitions at above 300 nm because the fibril sample is mainly composed of edge-sharing NbO$_6$ octahedra, which concurs with the XRD and the Raman results. For the 1% Ta^V doped sample, the intensity of the absorption at above 300 nm is the second highest because it was composed both of a fibre and of a bar-like solid. Other samples, especially the undoped ones, displayed weak absorption. These are mainly composed of intermediates with edge-sharing octahedra, and their absorption bands were observed at only ~250 nm. Furthermore, the spectra of pure niobate (0% Ta) showed the same evolution as the spectra obtained for 10% Ta mixed Nb oxides. An obvious shift of absorption bands can be seen for various concentration of Ta in the niobate matrix. This significant shift means that the presence of Ta within the niobate matrix not only influences the morphology of the products, but also has an effect both on the lattice structure and on the electronic properties.

3.4 Sorption of bivalence radioactive ions

Figure 4 illustrates the adsorption isotherms of Ba^{2+} and Sr^{2+} by various amounts of the tantalum doped niobate samples. For the removal of the Ba^{2+} ions (Figure 4a), the bar-like solids exhibited high sorption ability. For instance, the uptake capacities of Ba^{2+} ions by 0, 0.5, 5, and 10% Ta^V doped samples are quite similar and are ~ 470 mg/g. However, 2% of the Ta doped fibre phase sample displays weak sorption ability with its capacity being only ~ 220 mg/g. The uptake capacity of 1% Ta^V doped sodium niobate was composed of bar-like solids and few fibres are ~ 400 mg/g. For the removal of the Sr^{2+} ions, the bar-like solids also displayed a higher exchange capacity than the fibril one (Figure 4b). This is similar to the sorption of the Ba^{2+} ions.

For example, the uptake capacities of the Sr^{2+} of bar-like solids were doped with 0.5, 5, and 10% Ta^V are 250, 260, and 270 mg/g, respectively. The value of the pure sodium niobate solid is slightly less than 250 mg/g. This means that the availability of exchangeable Na^+ ions in poorly-crystallized bar-like solids is more than that of the well-crystallized fibres. The results presented above highlight the impact of tantalum in the framework design and the resulting morphological forms obtained after hydrothermal synthesis, which performed differently in the ion-exchange processes. Too much (10%) or too little (0% and 0.5%) tantalum in the reactions gives rise to solids which don't crystallize well. These less crystalline solids possess loosely held frameworks and therefore more ions are easily available for exchange reactions. Furthermore, the exchange of radioactive ions in the framework of weakly crystalline solids often imparts a high degree of apparently random rearrangement in the framework, which favours the encapsulation of radioactive ions irreversibly inside the framework. The sorption data leaves no doubt that the incorporation of Ta^V affecting the formation of the framework which can easily control the availability of the exchangeable Na^+ ions. Furthermore, the semi crystalline solids contribute more active adsorption sites for the exchange of radioactive sites.

The distribution coefficient, K_d, represents the ratio of the concentration of M^{2+} ions absorbed on one gram of various forms of niobate versus the concentration of M^{2+} left in solution (per milliliter) and is listed in Table 1. It can be observed that the bar-like solids doped with 0.5, 5, and 10% Ta^V exhibit higher K_d than those of the fibril one; this is due to the higher sorption capacities of the Ba^{2+} and Sr^{2+} ions. Furthermore, it is also noted that even in the presence of the sodium ions K_d remains significantly high for semi-crystalline solids. This is a succinct illustration of the fact that the semi-

crystalline solids have achieved optimum crystallinity in order to gain maximum selectivity for the removal of radioactive ions.

As seen in Figure 5, the exchange of radioactive ions was carried out in two different steps: 1) the hydration of the sodium ions that were present in the niobate crystals and that resulted is the formation of micelle 2) the hydrated Sr^{2+} and Ra^{2+} (Ba^{2+}) were exchanged with sodium ions due to its less tendency to form soluble products which creates products with less free energy. The property of permanently trapping the radioactive cations allows us to isolate the radioactive ions from the contaminated water, so that the tantalum doped sodium niobate and the used adsorbents can be disposed of safely without the risk of release of the adsorbed cations from the adsorbents that may cause secondary contamination. To ensure the binding of radioactive ions inside the niobate solids, we carried out a desorption test. The solid contents were separated out from aqueous solutions by using a centrifuge. The recovered solids were kept at 80 ^{o}C for 24 h. Water was then added to the solid samples and the dispersions were equilibrated in a shaker at room temperature for 48 h. The salt contents released into the water were analyzed by an ICP technique. This experiment revealed that bar-like solids showing a high level of leaching resistance from the framework. It was found that only $\sim$ 5% of the adsorbed M^{2+} ions were detected in the solution for the bar-like solids, indicating that $\sim$ 95% of the radioactive ions had been locked in the adsorbents. However, in the sample with fibril morphology, 90% of the adsorbed M^{2+} ions were detected in solution. This means that it is more feasible to use the bar-like solids as adsorbents in the removal of radioactive ions from water.

To uncover the large difference in the adsorption properties between the bar-like solids and the fibre adsorbents, we compared the XRD patterns and the Raman spectra of the Ta^V doped sodium niobates before and after sorption. The XRD patterns are shown in Figure 6. For the bar-like solids, the XRD patterns changed greatly after sorption (Figure a, b, e, and f). The most obvious variation is that the peaks between $2\theta = 20°$ and $60°$ disappeared or decreased significantly after the sorption of Ba^{2+} and Sr^{2+} ions. It is also noticeable that the peaks at $2\theta = 10°$ to $15°$ shifted to a low angle after sorption of Ba^{2+} ions. Although the structural change is too complicated to be analyzed in detail, we can determine that both the higher sorption capacity and the leaching resistance are due to the easily changed structure of the bar-like solids.

Because the bar-like solids are poorly-crystallized, the sodium ions in the solids can be more easily exchanged by the radioactive ions. After sorption, the structure of the metastable solids were either deformed or collapsed. This resulted in the radioactive ions being locked into the solids and not being released again. However, for the fibril solid, no structural change is observed after the sorption process (Figure 6d). As discussed in Figure 6, the fibre adsorbent is a well-crystallized solid. Therefore the sodium ions available for the exchange of Ba^{2+} or Sr^{2+} are relatively few compared to the quantity of bar like solids. The XRD signals obtained from the sample after the adsorption of radioactive ions were essentially identical to the corresponding fresh fibres. Furthermore, the crystal structures of the fibres were almost insensitive to the adsorption process, indicating that radioactive ions that were added were not involved in the framework rearrangement. Therefore the recovered radioactive ions were easily leached out from the framework. For the solid composed of bars and fibers, only the bar-like solids really adsorb the radioactive ions and the fibril solids are not strongly involved in this part of the absorption process. Therefore, the peaks that correspond to

the poorly-crystallized bar solids are changed after adsorption and the peaks that are assigned to the fibril phase still remain unchanged (Figure 6c). The Raman spectra provide similar results with the XRD pattern (Figure 7).

4. Conclusion

Sodium niobates doped with different amount of Ta^V (0, 0.5, 1, 2, 5, and 10%) were prepared via thermal reaction process. Pure nanofibril solids can be obtained when 2% Ta^V was introduced into the reaction system. These hybrid fibers are well-crystallized and are mainly composed of edge-sharing NbO_6 octahedra. Bar-like solids can be obtained under other conditions. These bar-like solids are poorly-crystallized and are mainly composed of intermediates with edge sharing $Nb_6O_{19}^{8-}$ units. It was observed that the bar-like solids possess high sorption capacities for bivalent radioactive ions, such as Sr^{2+} and Ra^{2+} (Ba^{2+}). And even though in presence of lots of Na^+ ions, the solids are able to selectively adsorb the bivalent radioactive ions. More importantly, considerable structure deformation or collapse occurs during the sorption process, resulting in entrapment of the dangerous bivalence cations in the solids. In particular, it is possible that a metastable framework rather than a rigid structure, which consequently enabled the solids to be suitable for concentrating most of the radionnuclides from contaminated water and would allow the bulk of the waste to be disposed of. Obviously, the newly prepared Nb-based adsorbents may develop new pathway to remove the toxic radioactive ions from contaminated water.

References

[1]	D.J. Yang, Z.F. Zheng, H.Y. Zhu, H.W. Liu, X.P. Gao, Advanced Materials 20 (2008) 2777.
[2]	S. Komarneni, N. Kozai, W.J. Paulus, Nature 410 (2001) 771.
[3]	W.J. Paulus, S. Komarneni, R. Roy, Nature 357 (1992) 571.
[4]	S. Komarneni, R. Roy, Nature 299 (1982) 707.
[5]	S. Komarneni, R. Roy, Science 239 (1988) 1286.
[6]	M. Nyman, A. Tripathi, J.B. Parise, R.S. Maxwell, W.T.A. Harrison, T.M. Nenoff, Journal of the American Chemical Society 123 (2001) 1529.
[7]	M. Nyman, A. Tripathi, J.B. Parise, R.S. Maxwell, T.M. Nenoff, Journal of the American Chemical Society 124 (2002) 1704.
[8]	P.K. Mohapatra, D.S. Lakshmi, A. Bhattacharyya, V.K. Manchanda, Journal of Hazardous Materials 169 (2009) 472.
[9]	T.P. Valsala, S.C. Roy, J.G. Shah, J. Gabriel, K. Raj, V. Venugopal, Journal of Hazardous Materials 166 (2009) 1148.
[10]	F. Belloni, C. Kuetahyali, V.V. Rondinella, P. Carbol, T. Wiss, A. Mangione, Environmental Science & Technology 43 (2009) 1250.
[11]	P. Sharma, R. Tomar, Microporous and Mesoporous Materials 116 (2008) 641.
[12]	A. Dyer, J. Newton, L. O'Brien, S. Owens, Microporous and Mesoporous Materials 120 (2009) 272.
[13]	M.J. Manos, N. Ding, M.G. Kanatzidis, Proceedings of the National Academy of Sciences of the United States of America 105 (2008) 3696.
[14]	P.K. Mohapatra, S.A. Ansari, A. Sarkar, A. Bhattacharyya, V.K. Manchanda, Analytica Chimica Acta 571 (2006) 308.
[15]	N. Rawat, P.K. Mohapatra, D.S. Lakshmi, A. Bhattacharyya, V. Manchanda, Journal of Membrane Science 275 (2006) 82.
[16]	D.L. Guerra, A.A. Pinto, R.R. Viana, C. Airoldi, Journal of Hazardous Materials 171 (2009) 514.
[17]	B.W. Mercer, L.L. Ames, P.W. Smith, Nuclear Applications and Technology 8 (1970) 62.
[18]	A. Dyer, A.M. Yusof, J. Inor. Nucl. Chem. 41 (1979) 1479.
[19]	C.B. Amphlett, L.A. McDonald, M.J. Redman, J. Inor. Nucl. Chem. 6 (1958) 220.
[20]	G.M. Bancroft, J.B. Metson, S.M. Kanetkar, J.D. Brown, Nature 299 (1982) 708.
[21]	E.A. Behrens, P. Sylvester, A. Clearfield, Environmental Science & Technology 32 (1998) 101.
[22]	H.W. Xu, M. Nyman, T.M. Nenoff, A. Navrotsky, Chemistry of Materials 16 (2004) 2034.
[23]	H.Y. Zhu, Z.F. Zheng, X.P. Gao, Y.N. Huang, Z.M. Yan, J. Zou, H.M. Yin, Q.D. Zou, S.H. Kable, J.C. Zhao, Y.F. Xi, W.N. Martens, R.L. Frost, Journal of the American Chemical Society 128 (2006) 2373.
[24]	M. Jurado-Vargas, M. Oliguín, E. Erdóñez-Regil, M. Miménez-Reyes, Journal of Radioanalytical and Nuclear Chemistry 218 (1997) 153.
[25]	R.G. Anthony, R.G. Dosch, D. Gu, C.V. Philip, Industrial & Engineering Chemistry Research 33 (1994) 2702.

[26]   V.J. Inglezakis, M.D. Loizidou, H.P. Grigoropoulou, Water Research 36 (2002) 2784.
[27]   B. Morosin, P.S. Peercy, Chemical Physics Letters 40 (1976) 263.
[28]   J.-M. Jehng, I.E. Wachs, Catalysis Today 8 (1990) 37.
[29]   S. Lanfredi, L. Dessemond, A.C.M. Rodrigues, Journal of the European Ceramic Society 20 (2000) 983.
[30]   F.J. Farrell, V.A. Maroni, T.G. Spiro, Inorganic Chemistry 8 (2002) 2638.
[31]   J.M. Jehng, I.E. Wachs, The Journal of Physical Chemistry 95 (2002) 7373.
[32]   M.N. Iliev, M.L.F. Phillips, J.K. Meen, T.M. Nenoff, Journal of Physical Chemistry B 107 (2003) 14261.
[33]   Y. Chen, J.L.G. Fierro, T. Tanaka, I.E. Wachs, The Journal of Physical Chemistry B 107 (2003) 5243.
[34]   J. Huuhtanen, M. Sanati, A. Andersson, S. Lars T. Andersson, Applied Catalysis A: General 97 (1993) 197.
[35]   G. Blasse, G.P.M. van den Heuvel, Materials Research Bulletin 7 (1972) 1041.
[36]   G. Blasse, L.G.J. De Haart, Materials Chemistry and Physics 14 (1986) 481.
[37]   M. Wiegel, M. Hamoumi, G. Blasse, Materials Chemistry and Physics 36 (1994) 289.
[38]   W.-J. Chun, A. Ishikawa, H. Fujisawa, T. Takata, J.N. Kondo, M. Hara, M. Kawai, Y. Matsumoto, K. Domen, The Journal of Physical Chemistry B 107 (2003) 1798.

List of Figures

Figure1. Niobate solids illustrated by the SEM images of the samples: (a) 0% Ta, (b) 0.5% Ta, (c) 1% Ta, (d) 2% Ta, (e) 5% Ta, and (f) 10% Ta.

**Figure 2.** XRD patterns (a) and Raman spectra (b) of Ta^V doped niobate specimen.

Figure 3. The DR – UV – Vis spectra of Ta^V doped sodium niobates

Figure 4. The isotherms of M^{2+} sorption by the Ta doped niobate samples: (a) Ba^{2+} and (b) Sr^{2+}.

Figure 5. Ion exchange assisted absorption of radioactive ions on the framework of niobate: (a) sodium niobate crystals; (b) hydrated sodium niobate crystals; (c) hydrated radioactive ions; (d) sodium ions exchanged with ratioactive ions.

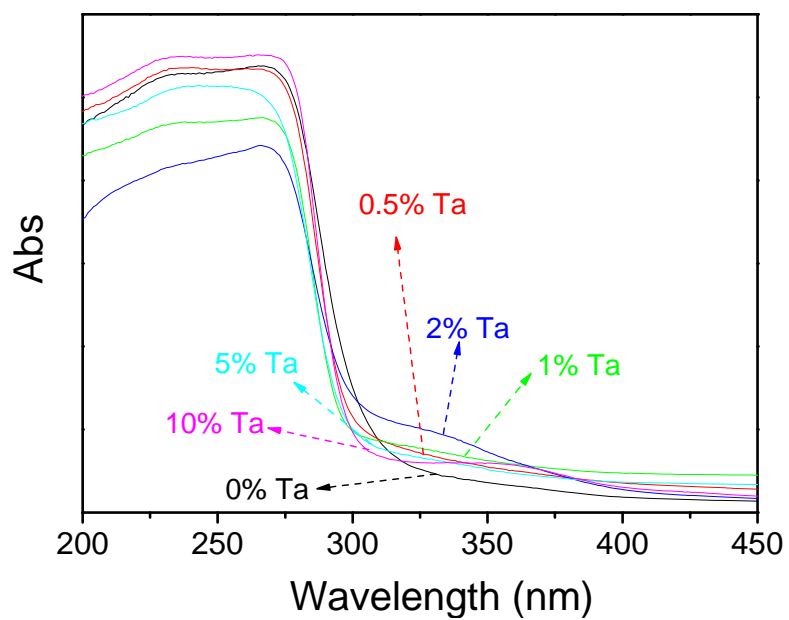**Figure 6.** The XRD patterns of the Ta^V doped sodium niobates before and after sorption of M^{2+} ions.

Figure 7. The Raman spectra of the Ta^V doped sodium niobates before and after sorption of M^{2+} ions.
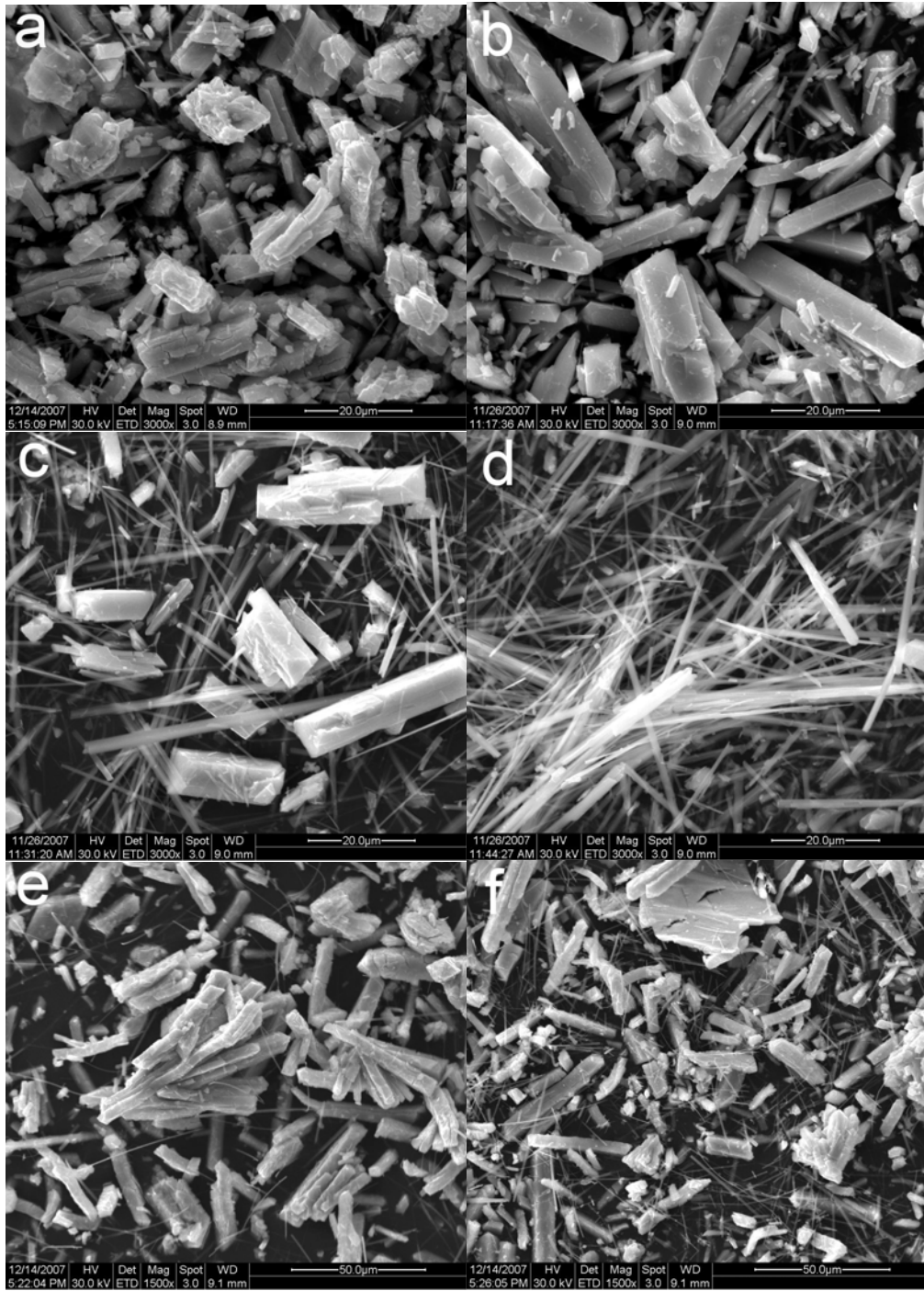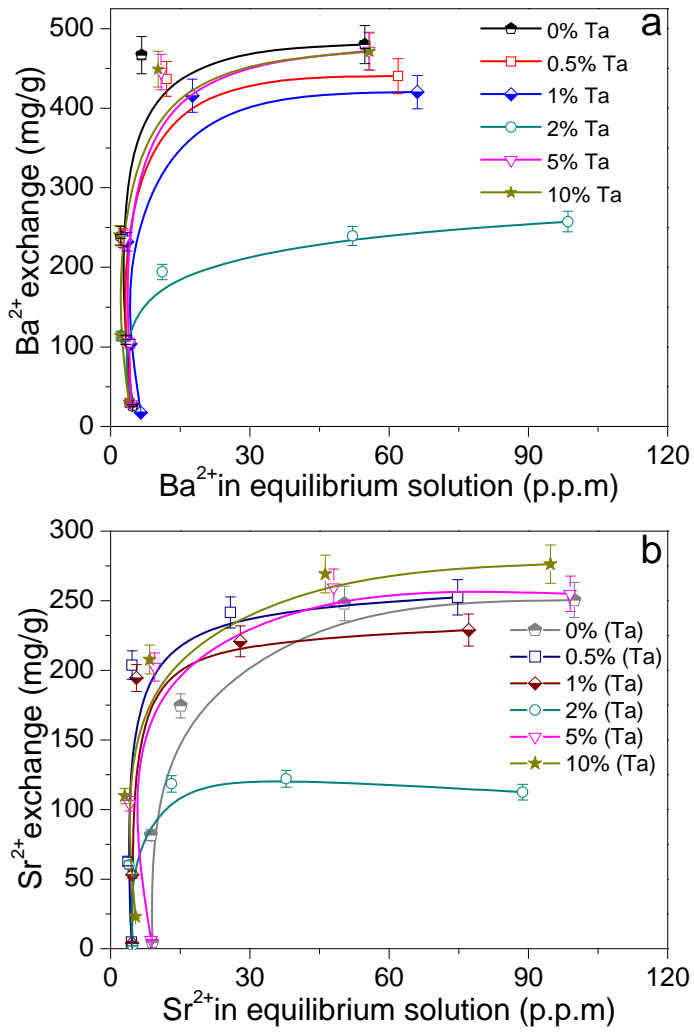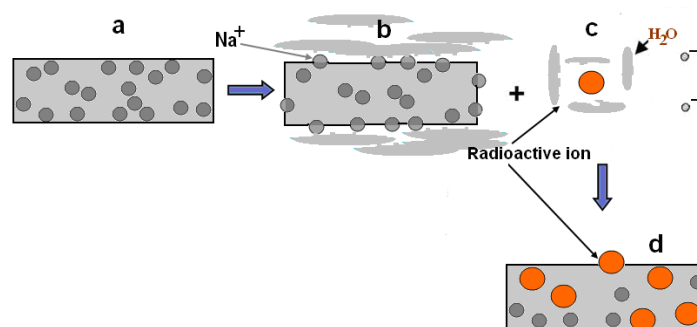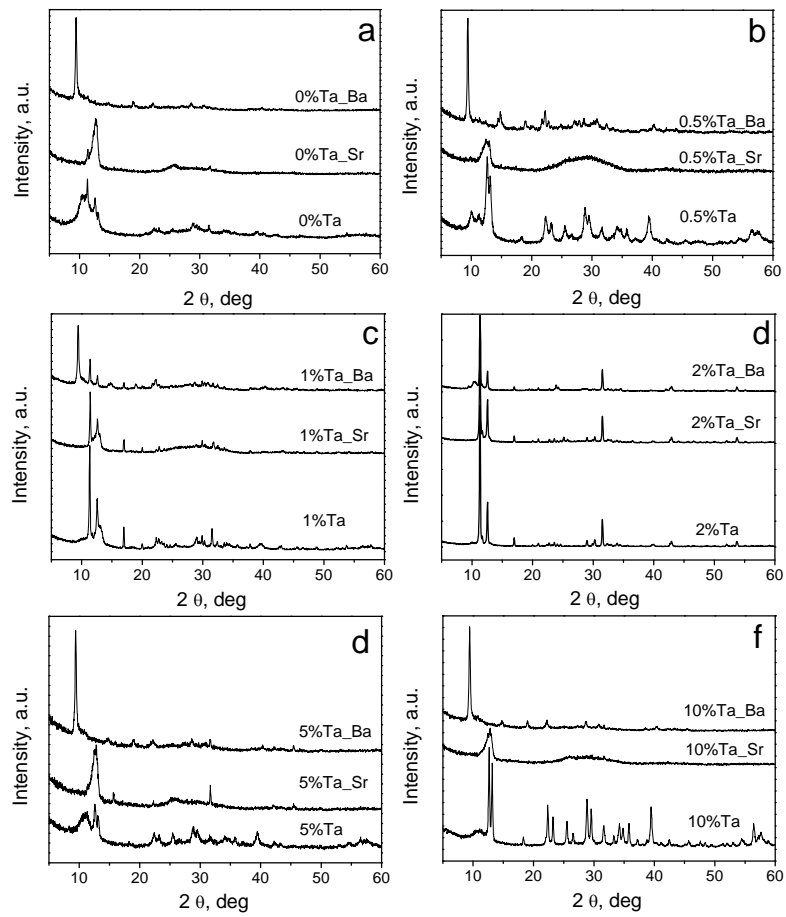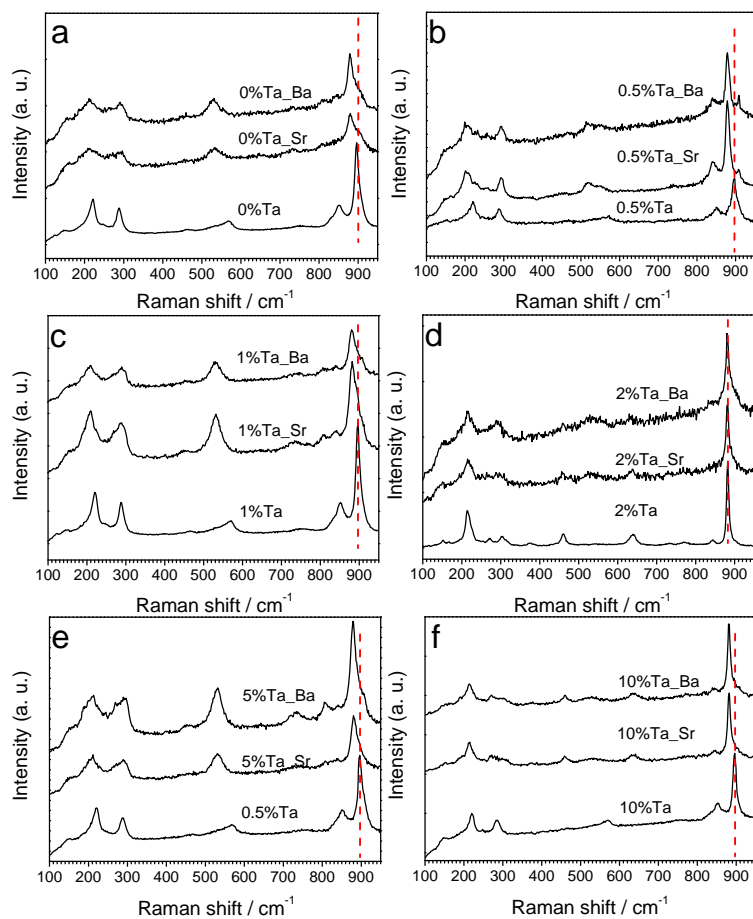
Figure1.
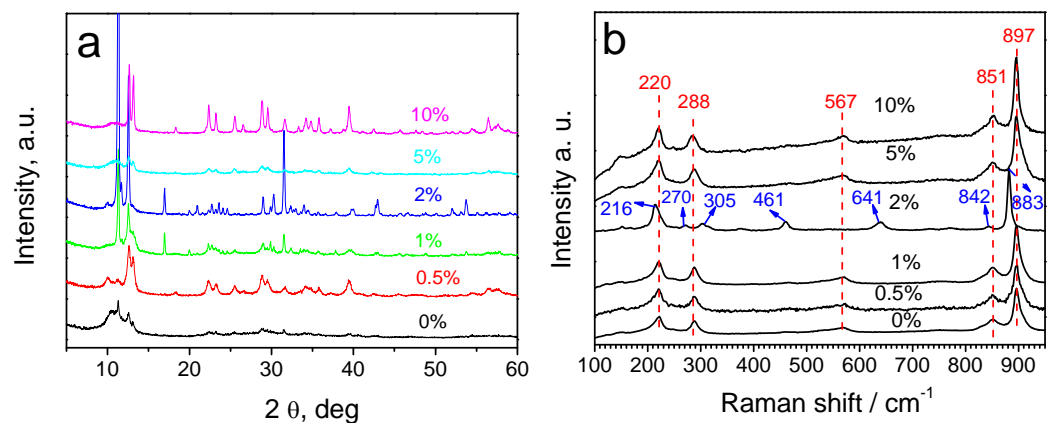
Figure 2.

Figure 3.

Figure 4.

Figure 5.

Figure 6.

Figure 7.

List of Tables

Table 1. K_d values for M^{2+} ion sorption by Ta^V doped sodium niobate adsorbents

C_{Na}*	0%-Ta^V		0.5%-Ta^V		1%-Ta^V		2%-Ta^V		5%-Ta^V		10%-Ta^V	
	Ba^{2+}	Sr^{2+}	Ba^{2+}	Sr^{2+}	Ba^{2+}	Sr^{2+}	Ba^{2+}	Sr^{2+}	Ba^{2+}	Sr^{2+}	Ba^{2+}	Sr^{2+}
0	45000	4842	39642	4724	18809	3928	1203	681	49347	5121	54323	5351
0.1	16860	3724	17087	3583	6034	3180	950	552	23498	3216	23705	3150

*C_{Na} is the concentration of NaCl in the solution of M^{2+} ions.